Available online at www.sciencedirect.com
SCIENCE DIRECT®
Journal of Chromatography A, 1059 (2004) 43–52
JOURNAL OF CHROMATOGRAPHY A
www.elsevier.com/locate/chroma

Adsorption of the enantiomers of 2,2,2-trifluoro-1-(9-anthryl)-ethanol on silica-bonded chiral quinidine-carbamate

Gustaf Götmar[a,b], Leonid Asnin[a,b], Georges Guiochon[a,b,*]

[a] *Department of Chemistry, The University of Tennessee, Knoxville, TN 37996-1600, USA*
[b] *Division of Chemical Sciences, Oak Ridge National Laboratory, Oak Ridge, TN, USA*

Received 22 July 2004; received in revised form 1 October 2004; accepted 4 October 2004

Abstract

The adsorption isotherms of the enantiomers of 2,2,2-trifluoro-1-(9-anthryl)-ethanol from a toluene–acetonitrile solution onto a *Chiris* Chiral AX:QD1 column were measured using the pulse method. The isotherm data were modeled with a bi-Langmuir isotherm model, indicating the presence of two different types of adsorption sites on this stationary phase, nonselective and enantioselective sites. The latter are homogeneous but interact with both enantiomers, albeit with different energies. The thermodynamic characteristics of these two types of sites were characterized by their adsorption constants and saturation capacities and by the influence of the temperature on these different parameters.

Keywords: Chiral stationary phase; Quinidine carbamate; Enantiomer separation; 2,2,2-Trifluoro-1-(9-anthryl)-ethanol

1. Introduction

In previous investigations, we have determined the competitive equilibrium isotherms of numerous pairs of enantiomers on different stationary phases, modeled these isotherms, discussed the retention mechanisms involved on the basis of the best isotherm models suggested by the experimental data, and compared the elution band profiles of various mixtures of these enantiomers with those calculated from appropriate chromatography models, using these isotherm equations. The compounds studied were the enantiomers of phenyl-alanine anilide (PA) on a polymer imprinted with L-PA [1] and of Fmoc-tryptophan on polymers imprinted with Fmoc-L-tryptophan [2]; of *N*-benzoyl alanine, leucine, tryptophan, 2-phenyl-propionic acid, 2-phenyl-butyric acid, and mandelic acid on BSA immobilized on silica or on an ion-exchange resin [3,4]; of propranolol, alprenolol, and metoprolol on the cellulase protein CBH I immobilized on porous silica [5,6]; of 1-phenyl-1-propanol, 3-chloro-1-phenyl-1-propanol, and 1-indanol on cellulose tribenzoate coated on porous silica [7–11]; Tröger's base on bulk cellulose triacetate [12] and on amylose tri-(3,5-dimethyl-phenyl carbamate) coated on porous silica [13,14]. A comparison between these sets of data and results provides some interesting conclusions regarding the behavior of the different chiral stationary phases (CSP) used [15]. These CSPs can be divided into two classes that exhibit markedly different adsorption behaviors.

The CSPs of the first class have two very different types of adsorption sites, the enantioselective and the nonselective sites. The former sites constitute a homogeneous group characterized by their narrow adsorption energy distribution, their significant distance, and their independence, as demonstrated by the small or negligible adsorbate–adsorbate interactions observed on these sites [16,17]. The latter sites correspond to the classical van der Waals, Keesom, and Dirac molecular interactions and simple hydrogen bonding which do not involve a chiral component. These sites have a broad energy distribution and a much lower average energy than the former

* Corresponding author. Tel.: +1 865 974 0733; fax: +1 865 974 2667.
E-mail address: guiochon@utk.edu (G. Guiochon).

0021-9673/$ – see front matter © 2004 Elsevier B.V. All rights reserved.
doi:10.1016/j.chroma.2004.10.025

sites; they are also far more numerous. To this class belong the imprinted polymers [1,2] and the immobilized proteins [3–6]. Adsorption of the template on the highly enantioselective, high-energy sites of the imprinted polymers is far stronger than that of its enantiomer, which provides a large chiral separation factor [1,2]. However, the development of an effective strategy for the separation of any pair of enantiomers remains hindered by the generally slow mass transfer kinetics observed with these CSPs [1]. Similarly, immobilized proteins contain high-energy adsorption sites that are highly enantioselective for one of the enantiomers of certain compounds [3–6]. This phenomenon is related to the presence of appropriate cavities inside the structure of active proteins. The molecules that can enter into these cavities and have the proper size and functional groups undergo strong interactions with the amino acid residues on the wall of the cavity, leading, under structurally favorable circumstances, to enantioselectivity and, thus, to chiral separations [6]. Unfortunately, several factors limit the generalization of the use of these CSPs. First, in almost all cases, there is only one cavity per protein molecule. This results in a low saturation capacity of this type of chiral columns and prevents their systematic use for preparative applications. Second, most of these CSPs are highly selective for only certain types of analytes. Finally, due to the high adsorption energy on the enantioselective sites, the mass transfer kinetics on these CSPs is often slow, particularly for the more retained enantiomer.

The interaction sites between the CSPs of the second class and the enantiomers have a much broader adsorption energy distribution. The distinction between enantioselective and nonselective sites does not seem to be possible anymore. The density of the enantioselective sites is much higher than the one found in CSPs of the first class and their saturation capacity is also much higher [7–14]. Probably, the chiral separation arises from the chiral environment surrounding the adsorbed molecules more than from specific interactions that would take place according to the classical three-point model [18]. Most of the CSPs of this class are derivatives of cellulose or amylose in which the quasi-totality of the OH groups have been reacted into low-polarity moieties. Although the mass transfer kinetics on these phases may not be much faster than it is on the CSPs of the first class, it seems controlled more by a slow diffusion throughout the polymeric network than by other factors since it corresponds to a low value of the diffusion coefficient [12].

It seems highly probable that CSPs made after the Pirkle model [18] should belong to the first type of CSPs. These phases are synthesized by bonding to silica a pure enantiomer of a chiral ligand selected for its ability to give enantioselective interactions which one of the enantiomers that need to be separated. So, we can expect to find enantioselective and nonselective sites on these CSPs, with the former sites being able to give labile complexes of markedly different Gibbs free energies with the two enantiomers while being remote enough to ensure that no adsorbate–adsorbate interactions take place. However, these sites cannot be shielded from each other on Pirkle CSPs as they are on proteins immobilized on a support. The relative heterogeneity of the silica surface may affect the structure of the bonded groups, hence the degree of heterogeneity of the adsorption energy distribution on the enantioselective sites. So far, no CSP of this class has been studied in detail. The goal of this work was to measure the adsorption isotherms of the enantiomers of a neutral compound on a Pirkle-type phase. We chose to investigate the retention and separation of the enantiomers of 2,2,2-trifluoro-1-(9-anthryl)-ethanol (TFAE) on a quinidine carbamate immobilized on a porous silica. This CSP is the relatively new representative of a family of chiral anion-exchangers that were developed for the enantioseparation of chiral acids [19,20]. There are so far no data sets in the literature that were acquired regarding the adsorption of neutral compounds on these types of sorbents. By contrast, the chromatographic behavior of TFAE and of other pairs of neutral enantiomers was studied on unsubstituted Chinchona alkaloids (e.g., quinine, quinidine, chinchonidine) [21–24].

2. Theory

The equilibrium isotherm data of the enantiomers of (*R*)- and (*S*)-2,2,2-trifluoro-1-(9-anthryl)-ethanol were determined (see later, Fig. 1), using a pulse method based on elution chromatography [25,26] and the inverse method [27].

2.1. The bi-Langmuir isotherm model

Examination of the experimental data (see later) showed that the best model accounting for the adsorption behavior of the compound studied in the phase system used was the bi-Langmuir model. Previous studies have shown that this isotherm model fits well the experimental data for many enantiomers adsorbed on CSPs of the first class [28–30]. The equation of the bi-Langmuir isotherm is

$$q = \frac{q_{ns} b_{ns} c}{1 + b_{ns} c} + \frac{q_s b_s c}{1 + b_s c} \quad (1)$$

where b_{ns} and b_s are the equilibrium constants for the adsorption on the nonselective and the enantioselective sites, respectively, q_{ns} and q_s are the saturation capacities for the nonselective and the enantioselective sites, respectively. The

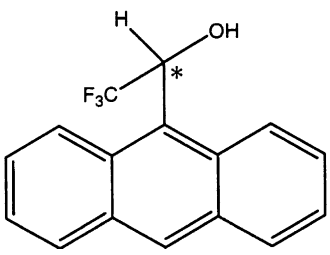

Fig. 1. Structure of 2,2,2-trifluoro-1-(9-anthryl)-ethanol; the chiral center is marked with an asterisk.

adsorption equilibrium constant, the enthalpy (ΔH_i), and the entropy (ΔS_i) of transfer of the solute from the liquid phase onto the adsorption sites of type i (i = n, ns) are related as follows

$$b = \exp\left(\frac{\Delta S_i}{R}\right)\exp\left(-\frac{\Delta H_i}{RT}\right), \quad (2)$$

For the sake of simplicity, in the following section, we will call these quantities the enthalpy and the entropy of the corresponding adsorption sites, respectively.

2.2. Determination of isotherm data

2.2.1. The pulse method

We used a modified Glueckauf method, as described in [31], in which sample pulses of increasing size are injected, after the column has been equilibrated with the mobile phase. To derive the adsorption equilibrium data, we used the following equation

$$\frac{\mathrm{d}q}{\mathrm{d}c} = \frac{V_\mathrm{R}(c) - V_0}{V_\mathrm{a}} = V'_\mathrm{R}(c) \quad (3)$$

where q is the adsorbed amount of solute at equilibrium of the stationary phase with a solution at a concentration c in the mobile phase, as calculated using a calibration curve, $V_\mathrm{R}(c)$ is the retention volume of the maximum of the peak, V_0 is the hold up volume of the column, and V_a is the volume of stationary phase in the column. Thus, the retention time of each peak gives one point on the V'_R versus c plot. By repeating the procedure while progressively increasing the volume of the sample, the set of data V'_R versus c is obtained, within the concentration range of interest. The amount adsorbed q is obtained by integration of the area under the function dq/dc, from 0 to c.

2.2.2. The inverse method

The inverse method of isotherm determination consists in calculating the numerical coefficients of an isotherm model so as to minimize the distance between an experimental overloaded band profile and the profile calculated with a suitable model of chromatography [27]. In most cases, the equilibrium-dispersive (ED) model of chromatography [26] is used. The differential mass balance equation is written:

$$\frac{\partial c}{\partial t} + \beta\frac{\partial q}{\partial t} + u\frac{\partial c}{\partial z} = D\frac{\partial^2 c}{\partial z^2} \quad (4)$$

where t and z are the time elapsed from the injection and the distance traveled by the band along the column, respectively; u is the interstitial mobile phase velocity; β is the phase ratio, defined as $\beta = (1-\varepsilon)/\varepsilon$, with ε being the total column porosity; and D is the apparent dispersion coefficient. D is evaluated through the well-known equation:

$$D = \frac{Hu}{2} \quad (5)$$

where H is the height equivalent to a theoretical plate.

The following initial and boundary conditions are used to solve Eq. (4).

- The initial condition correspond to a column that is empty of solute:

$$c(0, z) = 0; \quad (6)$$

- The boundary condition at the column inlet (at $t > 0$ and $z = 0$) is defined by the injection of a rectangular plug of solution:

$$c(t, 0) = \begin{cases} c_\mathrm{f} \text{ if } 0 < t < t_\mathrm{p} \\ 0 \text{ if } t_\mathrm{p} < t \end{cases} \quad (7)$$

  where t_p is the duration of the injection and the subscript f indicates an "inlet value".
- The boundary condition at the column outlet (at $t > 0$ and $z = L$; with L the column length) is:

$$\frac{\partial c}{\partial z} = 0 \quad (8)$$

The differential mass balance equation (Eq. (4)) was integrated by using the Rouchon algorithm [32].

2.3. Adsorption energy distribution

The theory of adsorption on heterogeneous surfaces considers that these surfaces are tiled with homogeneous patches, each one characterized by its own adsorption energy (E) and adsorption constant (b) [33]. Thus, there is a distribution of adsorption sites over a range of adsorption energies (AED) described by a function $F(E)$. By definition, this function is the derivative of the quantity of adsorption sites with respect to the adsorption energy and $F(E)\,\mathrm{d}E$ is the quantity of the sites that have an adsorption energy between E and $E + \mathrm{d}E$. To simplify the calculations, one assumes the AED to be continuous in the energy range from E_min and E_max. Then, the amount adsorbed at equilibrium with the concentration c of an adsorbate in solution is [33]

$$q(c) = \int_{E_\mathrm{min}}^{E_\mathrm{max}} \Theta(c, E)F(E)\,\mathrm{d}E \quad (9)$$

$\Theta(c, E)$ is the relative coverage of the adsorption sites with energy E. Sometimes, it is convenient to replace the distribution function of adsorption energies $F(E)$ by a distribution function of adsorption constants $F(b)$. E relates to b as (b_0 is the pre-exponential factor)

$$b = b_0 \exp\left(-\frac{E}{RT}\right) \quad (10)$$

where the ground state of an adsorbate in bulk solution is taken as the coordinate origin in the energy scale. (Note that, if we neglect the difference between the energy and the enthalpy, which is inessential in the condensed phase, the adsorption energy in Eq. (10) and the adsorption enthalpy will

be equivalent.) The adsorption isotherm on each homogeneous patch is considered to be the Langmuir isotherm, which yields for the overall adsorption isotherm with account of the transition to the *b*-scale:

$$q(c) = \int_{b_{\min}}^{b_{\max}} f(b) \frac{bc}{1+bc} \, \mathrm{d}(\ln b) \tag{11}$$

Localized adsorption takes place on the enantioselective sites, making this adsorption model obviously correct. In contrast, for the nonselective sites, the validity of the model is somewhat questionable. The problem is not only in that the adsorption on nonselective sites may be non-localized but also that the concept of nonselective part of the surface being made of a regular array of identical, well-defined geometrical sites, a concept that is necessary for the validity of the Langmuir isotherm model, is probably incorrect. The "supersites" approach [34], which treats the surface as a regular lattice of elements that are sufficiently large to hold several adsorbed molecules, seems to be more realistic for the description of the nonselective sites. However, this approach cannot be extended at present to the case of liquid/solid adsorption. Moreover, the classical model of heterogeneous surfaces described above has proven valid and appropriate for the interpretation of binding data to CPS's in a number of instances [17,30,35].

Obtaining numerical estimates of the AED of a CSP requires a numerical algorithm that inverts Eq. (9) to obtain $f(b)$ given only $q(c)$. We used in this work the iterative expectation-maximization method (EM), as described earlier [35,36]. This method protects better than most other methods of determination of the AED against the consequences of experimental artifacts which can be incorporated into the calculation of the AED. It operates from the raw adsorption data, without fitting them to an adsorption model. The EM method has been validated by showing the agreement between its numerical results and those of direct calorimetric measurements [37]. It has been successively used in the study of retention mechanisms on RPLC adsorbents [38,39].

3. Experimental

3.1. Equipment

All the measurements made in this work were carried out using a HP 1100 liquid chromatograph (Agilent Technologies, Palo Alto, CA), equipped with an automatic injector, a column oven, a variable wavelength detector, and a data acquisition system. The extra-column volume of this instrument was 0.131 ml. The mobile phase flow-rate was kept constant. It was set at 1 ml/min but the value measured by pumping the pure mobile phase into a 50 ml volumetric flask was actually 0.99 ml/min. We choose a wavelength of 330 nm to record the bands of TFAE and of 280 nm to record the peaks of 1,3,5-tri-*tert*-butyl-benzene (hold-up volume tracer). All the measurements were made at 22 °C, except when indicated specifically otherwise.

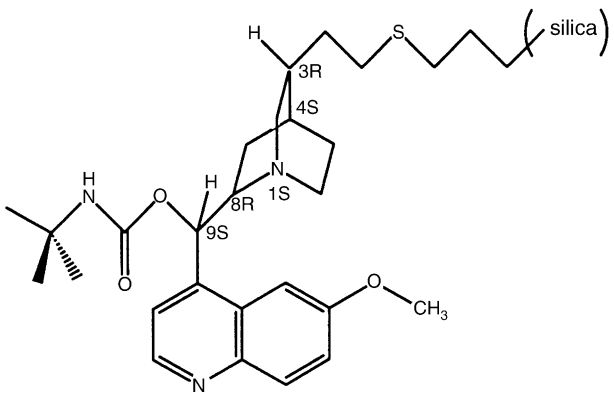

Fig. 2. Structure of the quinidine carbamate chiral selector.

3.2. Materials

3.2.1. Mobile phase and chemicals

The mobile phase was a toluene–acetonitrile solution (98:2, v/v). Both toluene and acetonitrile were HPLC grade solvents purchased from Fisher Scientific (Fair Lawn, NJ, USA). (*R*)- and (*S*)-2,2,2-trifluoro-1-(9-anthryl)-ethanol (structure in Fig. 1) and 1,3,5-tri-*tert*-butyl-benzene (TtBB) were from Aldrich (Milwaukee, WI, USA). All chemicals were used as supplied.

3.2.2. Column

The column used in this work was a 150 × 4 mm *Chiris* Chiral AX:QD1 column, from Iris Technologies (Lawrence, KS, USA). It was packed with approximately 1.2 g of 5 μm silica particles on the surface of which quinidine carbamate is immobilized. The structure of this ligand is illustrated in Fig. 2. The main characteristics of the packing material are summarized in Table 1.

3.3. Calibration

The calibration of the detector response was obtained using an indirect method described previously [40]. The calibration curve was calculated assuming that it is mildly nonlinear and given by a parabolic relationship

$$c = k_1' h + k_2' h^2 \tag{12}$$

where k_1' and k_2' are numerical coefficients. The coefficient k_1' was evaluated from the areas of the peaks recorded for

Table 1
Main characteristics of the stationary phase

Specific surface area (m^2/g)	300
Total pore volume (cm^3/g)	1
Average pore size (Å)	120
Bonding density (mmol/l)	590

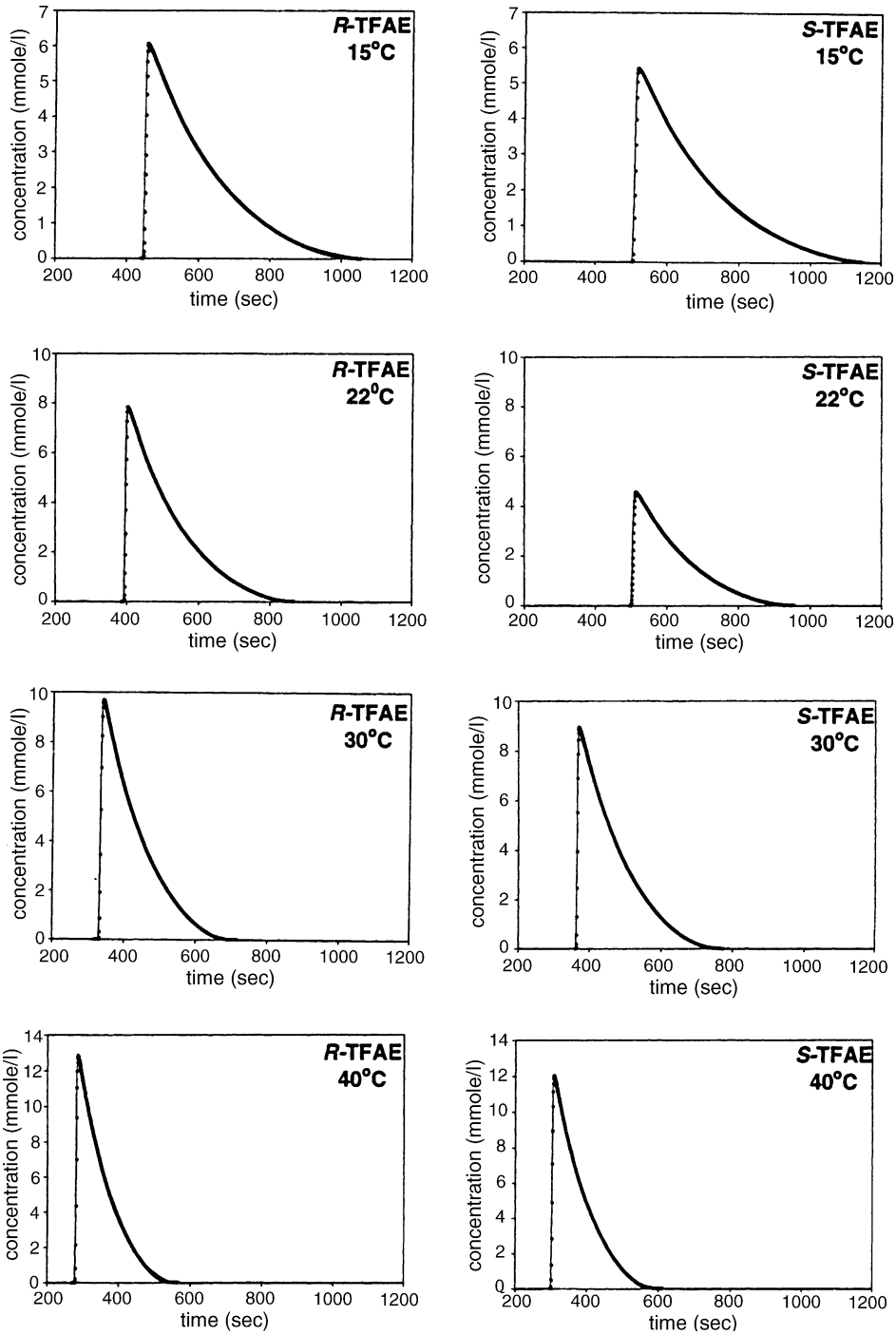

Fig. 3. Comparison between the calculated (solid line) and the experimental (circles) band profiles.

small amounts of sample (10 μl of dilute sample solutions of known concentrations), as

$$k_1' = \frac{q}{vS} \tag{13}$$

where q is the amount injected, v is the flow-rate of the mobile phase, and S is the area under the elution peak. To determine the value of k_2', data were acquired for larger amounts, by injecting 100 μl volumes of sample solutions. These data were fitted to Eq. (12), using the optimization procedure described earlier [40]. The method was validated by comparing the amounts injected and calculated from the calibration curve, for a series of samples, in the range of amounts injected between 0.5 and 5 mg (with 10 or 100 μl samples). The agreement between the injected and the calculated amount was always better than 2% in the whole range of amounts used. The error is estimated from the discrepancy between the calibration curves obtained for the *R*- and the *S*-enantiomers, curves

Table 2
Numerical coefficients of the isotherm (Eq. (1))

T (°C)	q_{ns} (mmol/l)	R.S.D. (%) (q_{ns})	b_{ns} (l/mmol)	R.S.D. (%) (b_{ns})	q_s mmol/l	R.S.D. (%) (q_s)	b_s (l/mmol)	R.S.D. (%) (b_s)	Total S.D.
(*R*)-TFAE									
15	262	0.04	0.0601	0.3	6.7	1.5	0.955	1.5	0.19
22	299	0.43	0.0431	0.5	6.5	1.5	0.662	1.5	0.25
22[a]	*367*		*0.0365*		*8.4*		*0.57*		
30	318	0.63	0.0307	0.7	9.9	2.0	0.342	1.5	0.27
40	355	0.56	0.0203	0.5	13.4	1.5	0.233	1.3	0.32
(*S*)-TFAE									
15	282	0.32	0.0614	0.33	8.00	1.3	0.843	1.1	0.16
22	293	0.51	0.0483	0.52	8.17	1.2	0.542	1.3	0.13
22[a]	*460*		*0.0290*		*13.4*		*0.477*		
30	327	0.83	0.0312	0.83	15.8	1.9	0.264	1.1	0.27
40	359	0.72	0.0224	0.71	13.6	1.9	0.191	1.9	0.31

[a] The values in italics are calculated from the AED data.

that should be identical since the two enantiomers have identical response factors for the UV-detector. This difference was always less than 3%.

3.4. Isotherm determination

The adsorption isotherms of both enantiomers were measured using the pulse method. The experimental data were collected in two groups. The first one was obtained with a 5 g/l solution, injecting volumes between 5 and 100 μl, and acquiring five data points. The second group was performed with a 50 g/l solution, injecting 10–100 μl samples, and acquiring seven data points. The calibration function $c(h)$ was determined as described in section 3.3 and used to calculate the equilibrium concentrations corresponding to given V_R. The hold-up time was measured as the retention time of the unretained TtBB, immediately after each series of experiments.

To calculate the parameters of the adsorption isotherm by the inverse method, the solution with concentration 50 g/l was used. The experiments were carried out at 15, 22, 30 and 40 °C. The sample volume was 100 μl, except in the case of (*S*)-TFAE at 22 °C when it was 60 μl. The conversion of the experimental band profiles recorded as UV-absorbance versus time into the concentration band profile was accomplished using the calibration function $c(h)$. Each band profile was recorded twice and in each case a practically perfect coincidence was observed between the two profiles.

4. Results and discussion

4.1. Isotherm data

Fig. 3 compares the experimental band profiles (symbols) and the best profiles calculated (lines) when determining the coefficients of the bi-Langmuir isotherm (Eq. (1)) model, using the inverse method. The two sets of profiles are overlaid within the graphic resolution of the figure, showing an excellent agreement and demonstrating the validity of the isotherm coefficients obtained. These coefficients are reported in Table 2. To further validate the inverse method and confirm the validity of the results, under our experimental conditions, Fig. 4 compares the adsorption isotherms obtained for both enantiomers at 22 °C with the pulse method and with the inverse method. There is a very good agreement between the results of these two methods. Another confirmation is given by the good agreement between the values of the initial slope of the isotherm and of the adsorption coefficient (K) measured under linear conditions [24], values compared in Table 3.

4.2. Adsorption energy distribution (AED)

The equilibrium isotherm data measured by pulse method at 22 °C were used to calculate the AEDs of the two enantiomers (13 and 11 experimental data points were acquired for (*R*)- and (*S*)-TFAE, respectively, see Section 3). The energy space was divided into 150 intervals. The calculations were executed starting with a number of iterations $N = 10^5$ and then increasing successively tenfold, until a stable AED function was obtained, at $N = 10^7$ and 10^8. The AED functions obtained are reported in Fig. 5. The quantitative charac-

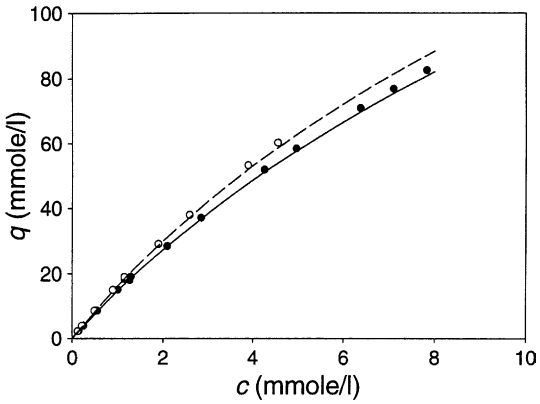

Fig. 4. Experimental isotherms measured by pulse method (solid circles for (*R*)-, open circles for (*S*)-TFAE) and best bi-Langmuir isotherms calculated by the inverse method (solid line for (*R*)-, dashed line for (*S*)-TFEA).

Table 3
Comparison of the adsorption constants at zero concentration obtained from measurements made under linear and nonlinear conditions

T (°C)	(*R*)-TFAE		(*S*)-TFAE	
	Initial slope	K[a]	Initial slope	K[a]
15	22.1	20.2	24.1	23.1
22	17.2	16.3	18.6	18.4
30	13.1	12.9	14.4	14.4
40	10.3	9.8	10.6	10.8

[a] $K = k'/\beta$ (k' is the capacity factor the values of which are discussed elsewhere [24]; β values were measured at each temperature with TtBB as the unretained tracer and are 0.53, 0.55, 0.56 and 0.58 at 15, 22, 30, and 40 °C, respectively).

teristics of the two distributions are compared in Table 2. For both enantiomers, a bimodal energy distribution is obvious. However, probably because the number of experimental data points was insufficient, significant differences are observed between the isotherm coefficients derived from the calculated AEDs and from the fits of the same data to the bi-Langmuir model. The saturation capacities calculated by integration of the corresponding peak of each AED are notably higher than those derived from the best bi-Langmuir coefficients, although the ratios q_{ns}/q_s for both enantiomers obtained with both methods coincide within 4%. The equilibrium constants b_{ns} and b_s derived from the AED are slightly shifted from the bi-Langmuir ones, both b_{ns} and b_s for (*R*)-TFAE being a little higher than for (*S*)-TFAE. The energy difference between the two types of sites for the two enantiomers is about 7 kJ/mol, close to the value found via the bi-Langmuir coefficients, following the equation

$$E_s - E_{ns} = RT \times [\ln(b_s) - \ln(b_{ns})] \quad (14)$$

This relationship is written assuming that the entropies of adsorption on the selective and the nonselective sites are equal, which is quite a reasonable approximation in view of the data in Table 4.

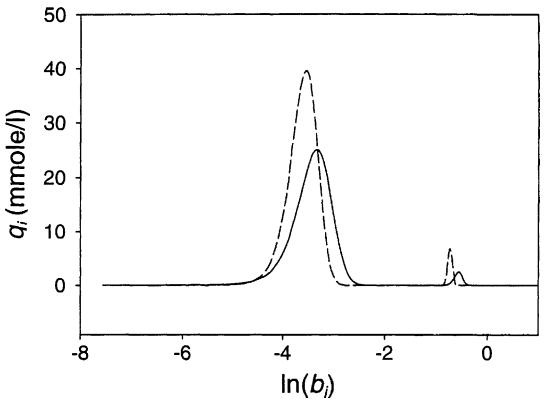

Fig. 5. Adsorption energy distribution of (*R*)-TFAE (solid line) and (*S*)-TFAE (dashed line). q_j is the concentration of adsorption sites with adsorption constant in the range $\ln b_j \pm \Delta \ln b_j$; $\Delta \ln b_j = 0.0584$.

Table 4
Thermodynamic characteristics of the adsorption sites according to the bi-Langmuir model

	(*R*)-TFAE	(*S*)-TFAE
$-\Delta H_s$ (kJ/mol)	43.9	46.4
$-\Delta H_{ns}$ (kJ/mol)	32.3	31.2
ΔS_s (J/mol K)	−152	−163
ΔS_{ns} (J/mol K)	−136	−131

4.3. Isotherm model

The theoretical background for the use of the bi-Langmuir isotherm in this case is that the CSP used in this work is expected to belong to the first class of CSPs, having on its surface two different types of adsorption sites, enantioselective and nonselective sites. The nonselective sites should retain as much either enantiomer, through conventional molecular interactions, whereas the enantioselective sites interact differently with the two enantiomers, binding them with different energies. The bonded ligand of the CSP studied has four chiral C-atoms and one chiral N-atom (see Fig. 1). A priori, each of these five chiral centers could be involved in the enantioselective adsorption sites, leaving the theoretical possibility of five different types of such sites. It is therefore an important result that the bi-Langmuir model fits the experimental data extremely well, as shown both by the bimodal character of the AED obtained and by the modeling of the adsorption isotherm data that fit excellently to the bi-Langmuir model. As shown in independent investigations, our methods can easily distinguish whether the best isotherm model is a bi-Langmuir, a tri-Langmuir, or a quadri-Langmuir model [41]. Therefore, this negative result is meaningful. One of the chiral center of the ligand (or possibly two but then acting in cooperation) is responsible for most, if not all the enantioselectivity of the CSP.

4.3.1. Nonselective sites

Although the isotherm data of both enantiomers were acquired and modeled separately, the numerical values obtained for the constant q_{ns} and b_{ns} are, within a few percent, the same for both enantiomers, as expected, with the only exception of the data at 15 °C for which the difference is slightly larger. The difference between the profiles of the low-energy mode of the AEDs of the two enantiomers is largely due to the inaccuracy of the results of the calculation caused by the small number of data points acquired.

4.3.2. Enantioselective sites

The values of the coefficients q_s and b_s are less different than is usual with CSPs of the first class but they are consistent with the small separation factor, of the order of 1.1 (calculated as ratio of the initial slopes in Table 3). It is common that the enantioselective sites of these CSPs do not interact with the least retained enantiomer. There are two possible explanations for the behavior of *Chiris* phase. Either there is only one type of enantioselective sites that interact differ-

ently with both enantiomers but to a significant degree with either, or there are two types of enantioselective sites, each one selective of a different enantiomer, and with a different interaction constant. Since the bonded groups have five chiral centers, this second possibility cannot be ruled out easily.

The comparison of the values of the saturation capacities for the two types of sites shows that the number of nonselective sites is much larger than that of the enantioselective sites. Taking the relatively high density of the bonded phase into account, one can suppose that not all of the chiral centers work as enantioselective adsorption sites. An approximate estimate based on the saturation capacities of the bi-Langmuir isotherm (Table 2), shows that the saturation capacity of the enantioselective sites corresponds to the adsorption of approximately 0.015 molecule of TFAE per bonded ligand. This value is surprisingly small. It could be explained only by a considerable hindrance of the chiral group responsible for enantioselectivity. In contrast, the saturation capacity of the nonselective site is of the order of half the number of bonded ligands but there are, obviously, no reasons for the nonselective interactions to involve only these ligands.

It is interesting to note that the two saturation capacities (both q_{ns} and q_s) increase with increasing temperature. This may be explained by the corresponding decrease of the extent of the solvation of the stationary phase surface by the mobile phase molecules at more elevated temperatures. Indeed, a decrease of the fraction of the surface area occupied by one component (in this case, the solvent) results in an increase of the fraction of this area occupied by the other component (the solute), due to the competitive nature of liquid/solid adsorption.

Finally, the interaction energy with the high-energy sites is practically the same for both enantiomers (Fig. 5). The enantioselectivity of the *Chiris* phase is due, not to a difference in interaction energy between the two enantiomers and the enantioselective sites, but to the difference between the saturation capacities of these sites for the two enantiomers. A similar observation has been made for the separation of the enantiomers of propranolol on immobilized Cel 7A [16]. In this latter case, both the adsorption constant and the saturation capacity of the high-energy sites depended on the buffer pH.

4.4. Isosteric heats of adsorption

The differential molar enthalpy of adsorption (i.e., the enthalpy of transfer of the solute from the mobile to the stationary phase) in the case of binary solution is given by [43]

$$-\Delta\bar{H}_{st} = RT^2\left(\frac{\partial \ln a}{\partial T}\right)_{\pi,q,q_2} \quad (15)$$

where π is the spreading pressure, a is the activity of the solute in the solution, q and q_2 are the surface excesses of the solute and the solvent, respectively. This equation requires that the ratio q/q_2 be independent of the temperature, which is generally not true. Moreover, the equation contains the activity of the solute, not its concentration. Parfitt and Rochester [43] have pointed out that "the use of the Clapeyron–Clausius equation to obtain the heats of adsorption from the adsorption isotherms which represent the interfacial excess of only one component at different temperatures can give misleading results". In other words, the quantity defined by the following equation (i.e., Eq. (16)), which is usually called the "isosteric heat of adsorption," has no strict thermodynamical sense.

$$Q_{st} = RT^2\left(\frac{\partial \ln c}{\partial T}\right)_q \quad (16)$$

Nevertheless, this quantity reflects undoubtedly some of the thermodynamic properties of the adsorption equilibrium and Q_{st} approaches $-\Delta\bar{H}_{st}$ when q decreases toward zero. However, it is necessary to take into account the restrictions reported above and to use most carefully the numerical values of Q_{st} for an analysis of the adsorption behavior.

The numerical data on the relationship between Q_{st} and q are reported in Table 4. The values obtained are positive, indicating that the adsorption is exothermic. The value of the isosteric heat of adsorption for small amounts adsorbed are in good agreement with those derived from experiments made under linear conditions [24], which were 20.4 and 19.2 kJ/mol for the (*S*)- and the (*R*)-enantiomer, respectively. The values obtained in the present case are about 3 kJ/mol larger. The difference between the isosteric heats of adsorption of the two enantiomers is close to 1 kJ/mol, as for the linear experiment data. This difference does not change as q increases. The numerical values obtained are of the same order of magnitude as the heats of adsorption observed for TFAE in RPLC with methanol–water solvents [42]; these values are rather higher than for a C_{18} stationary phase (12 kJ/mol) but lower than for β-cyclodextrin one (34 kJ/mol).

The values of for both enantiomers decrease with increasing value of q. Such a trend is usually explained by an energetically heterogenous surface of the adsorbent [33]. However, there are other possible reasons that could affect this trend, for example adsorbate–adsorbate interactions or deviations of the liquid phase from ideal behavior when its concentration increases. In principle, the former are certainly possible at high surface coverage, because the molecules of TFAE have a hydroxyl group and are able to undergo H-binding interactions with each other. However, when there are significant adsorbate–adsorbate interactions, the best isotherm model is a Moreau or a bi-Moreau isotherm [35], which does not take place in this case.

Fig. 6 shows a van't Hoff plot of b_i versus T. From this graphs, it is possible to derive the average thermodynamic parameters of each type of adsorption sites (Eq. (2)), parameters given in Table 5. The scatter of the data points pertaining to the selective sites is somewhat larger than that corresponding to the nonselective sites. However, the correlation coefficients are still larger than 0.98, which suggests that the temperature coefficients of the constants b make physical sense. The dif-

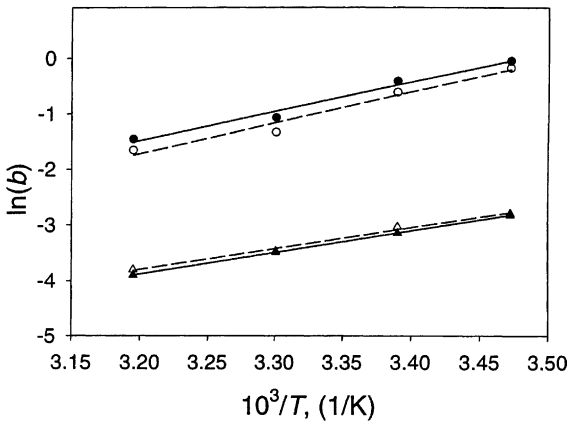

Fig. 6. Temperature dependence of the bi-Langmuir adsorption constants b_s (circles) and b_{ns} (triangles); open symbols belong to (*S*)-TFAE, black symbols belong to (*R*)-TFAE. Solid and dashed lines correspond to (*R*)- and (*S*)-enantiomer, respectively.

Table 5
Amount adsorbed and isosteric heat of adsorption

q (mmol/l)	Q_{st} (*R*) (kJ/mol)	Q_{st} (*S*) (kJ/mol)
5	22.5	23.6
10	21.7	22.9
50	19.6	20.4
70	18.9	19.8

ference between the adsorption enthalpies on the enantioselective and the nonselective sites is about 10 kJ/mol. The values measured for the enthalpy of adsorption on both sites are higher than those obtained for the isosteric heat of adsorption, for both enantiomers. This may be explained by the fact that the adsorption enthalpies are derived from *b*. Accordingly, they are probably related to the most active of the adsorption sites whereas Q_{st} is the result of an averaging process taking place over all the possible adsorption sites.

5. Conclusions

The results presented demonstrate that the CSP *Chiris* Chiral AX:QD1 belongs to the first class of CSPs. The adsorption data acquired fit well to a bi-Langmuir isotherm while the adsorption energy distribution is bimodal. This shows that retention takes place through two types of interaction sites, high-energy enantioselective and low-energy nonselective sites, the energy of the former being 7–10 kJ/mol higher than that of the latter sites for the molecular probe (TFAE) used in this work. The number of nonselective sites is 30–40 times higher than the number of enantioselective sites. However, the difference in energy is sufficient to allow for the separation of the two enantiomers at low or moderate concentrations. The positive values of the isosteric heats of adsorption indicate that the retention process is exothermic, as it is usual in LC systems involving only a small number (1–2) of hydrogen bonds and of polar van der Waals interactions.

Acknowledgments

This work was supported in part by Grants of the US Department of Energy and National Science Foundation and by the cooperative agreement between the University of Tennessee and Oak Ridge National Laboratory. We thank Wolfgang Lindner, University of Vienna, Austria, for fruitful discussions.

References

[1] Y. Chen, M. Kele, B. Sellergren, G. Guiochon, J. Chromatogr. A 927 (2001) 1.
[2] H. Kim, G. Guiochon, Anal. Chem., in press.
[3] S.C. Jacobson, S. Golshan-Shirazi, G. Guiochon, J. Am. Chem. Soc. 112 (1990) 6492.
[4] S.C. Jacobson, S. Andersson, S.G. Allenmark, G. Guiochon, Chirality 5 (1993) 513.
[5] T. Fornstedt, G. Zhong, Z. Bensetiti, G. Guiochon, Anal. Chem. 68 (1996) 2370.
[6] T. Fornstedt, G. Guiochon, Anal. Chem. 73 (2001) 608A–617A.
[7] A. Cavazzini, K. Kaczmarski, P. Szabelski, D. Zhou, X. Liu, G. Guiochon, Anal. Chem. 73 (2001) 5704.
[8] A. Cavazzini, A. Felinger, K. Kaczmarski, P. Szabelski, G. Guiochon, J. Chromatogr. A 953 (2002) 55.
[9] D.E. Cherrak, S. Khattabi, G. Guiochon, J. Chromatogr. A 877 (2000) 109.
[10] D. Zhou, D.E. Cherrak, A. Cavazzini, K. Kaczmarski, G. Guiochon, Chem. Eng. Sci. 58 (2003) 3257.
[11] D. Zhou, K. Kaczmarski, A. Cavazzini, X. Liu, G. Guiochon, J. Chromatogr. A 1020 (2003) 199.
[12] A. Seidel-Morgenstern, G. Guiochon, Chem. Eng. Sci. 48 (1993) 2787.
[13] K. Mihlbachler, K. Kaczmarski, A. Seidel-Morgenstern, G. Guiochon, J. Chromatogr. A 955 (2002) 35.
[14] K. Mihlbachler, A. Seidel-Morgenstern, G. Guiochon, AIChE J. 50 (2004) 611.
[15] T. Fornstedt, P. Sajonz, G. Guiochon, Chirality 10 (1998) 375.
[16] T. Fornstedt, G. Götmar, M. Andersson, G. Guiochon, J. Am. Chem. Soc. 121 (1999) 1164.
[17] G. Götmar, B.J. Stanley, T. Fornstedt, G. Guiochon, Langmuir 19 (2003) 6950.
[18] W.H. Pirkle, T.C. Pochapsky, Chem. Rev. 89 (1989) 347.
[19] A. Mandl, L. Nicoletti, M. Lämmerhofer, W. Lindner, J. Chromatogr. A 858 (1999) 1.
[20] M. Lämmerhofer, W. Lindner, J. Chromatogr. A 741 (1996) 33.
[21] P. Salvadori, C. Rosini, D. Pini, C. Bertucci, P. Altemura, G. Uccello-Barretta, A. Raffaelli, Tetrahedron 43 (1987) 4969.
[22] P.N. Nesterenko, V.V. Krotov, S.M. Staroverov, J. Chromatogr. A 667 (1994) 19.
[23] P.N. Nesterenko, V.V. Krotov, S.M. Staroverov, Zh. Fiz. Khim. 65 (1991) 2671.
[24] L. Asnin, G. Götmar, G. Guiochon, J. Chromatogr. A, submitted for publication.
[25] E. Glueckauf, Trans. Faraday Soc. 51 (1955) 1540.
[26] G. Guiochon, S.G. Shirazi, A.M. Katti, Fundamentals of Preparative and Nonlinear Chromatography, Academic Press, Boston, MA, 1994.
[27] F. James, M. Sépúlvéda, F. Charton, I. Quiñones, G. Guiochon, Chem. Eng. Sci. 54 (1999) 1677.
[28] A. Felinger, D. Zhou, G. Guiochon, J. Chromatogr. A 1005 (2003) 35.
[29] G. Götmar, T. Fornstedt, M. Andersson, G. Guiochon, J. Chromatogr. A 905 (2001) 3.

[30] G. Götmar, D. Zhou, B.J. Stanley, G. Guiochon, Anal. Chem. 76 (2004) 197.
[31] S.N. Lanin, M.Yu. Ledenkova, Yu.S. Nikitin, Mendeleev Commun. 10 (2000) 37.
[32] P. Rouchon, M. Shonauer, P. Valentin, G. Guiochon, Sep. Sci. Technol. 22 (1987).
[33] M. Jaroniec, R. Madey, Physical Adsorption on Heterogeneous Solids, Elsevier, Amsterdam, 1988.
[34] E. Bottani, W.A. Steele, Adsorption 5 (1999) 81.
[35] B.J. Stanley, P. Szabelski, Y.-B. Chen, B. Sellergren, G. Guiochon, Langmuir 19 (2003) 772.
[36] B.J. Stanley, G. Guiochon, J. Phys. Chem. 97 (1993) 8098.
[37] G. Götmar, G. Guiochon, Langmuir 20 (2004) 6521.
[38] F. Gritti, G. Guiochon, Anal. Chem. 75 (2003) 5726.
[39] F. Gritti, G. Guiochon, Anal. Chem. 76 (2004) 4779.
[40] E.V. Dose, G. Guiochon, Anal. Chim. 62 (1990) 816.
[41] F. Gritti, G. Guiochon, J. Chromatogr. A 1021 (2003) 25.
[42] Z. Chen, T. Nakayama, T. Nakagama, K. Uchiyama, T. Hobo, J. Liq. Chromatogr. 26 (2003) 2809.
[43] G.D. Parfitt, C.H. Rochester, Adsorption From Solution at the Solid/Liquid Interface, Academic Press, London, 1983.